Materials and Methods

Imaging

Quantitative analysis

Machine learning and pattern recognition techniques have proven extremely useful for various medical image analysis workflows (see, for example, the annual Workshop on Machine Learning in Medical Imaging held in conjunction with the Medical Image Computing and Computer-Aided Intervention international meeting [1]). Popular techniques such as support vector machines and neural networks have been applied successfully to clinically relevant imaging tasks such as segmentation (e.g., [2]) and diagnostic prediction (e.g., [3, 4]).

Another versatile technique that has acheieved much success

The random forest machine learning framework provides an excelllent fromework for medical image segmentation

Supervised methodologies are uniquely characterized, in part, by the feature images that are used to identify the regions of interest.

Intensity information alone is insufficient for removing false positives. For example, as pointed out in [5], higher intensities can be found at the periventricular caps in normal subjects which often confounds automated lesion detection algorithms.

To calculate this quantity for a single feature from a single random forest model, the decrease in prediction accuracy produced by omitting the specified feature is calculated during the out-of-bag phase of model creation.

During the out-of-bag error calculation stage of the random forest model creation, the decrease in prediction accuracy with the omission of a single feature or variable is tracked and averaged. Those features which have the greatest decrease in mean accuracy are considered to be the most discriminative. In this work, we do not use these measurements for feature pruning.

Feature type	Image source
Intensities	
normalized/preprocessed	FLAIR, T1, and T2
Symmetric template	
template difference	FLAIR, T1, and T2
contralateral difference	FLAIR, T1, and T2
location indices	FLAIR, T1, and T2
Segmentation probabilities	
Pr(cerebrospinal fluid)	T1
Pr(gray matter)	T1
Pr(white matter)	T1
Pr(deep gray matter)	T1
Pr(brain stem)	T1
Pr(cerebellum)	T1
Distance maps	
cerebrospinal fluid	T1 brain segmentation
gray matter	T1 brain segmentation
deep gray matter	T1 brain segmentation
whole brain	T1 brain segmentation
Neighborhood statistics	
mean	FLAIR, T1, and T2
standard deviation	FLAIR, T1, and T2
skewness	FLAIR, T1, and T2

Table 1: List of feature images used for Stage 1 of the proposed white matter hyperintensity segmentation framework.

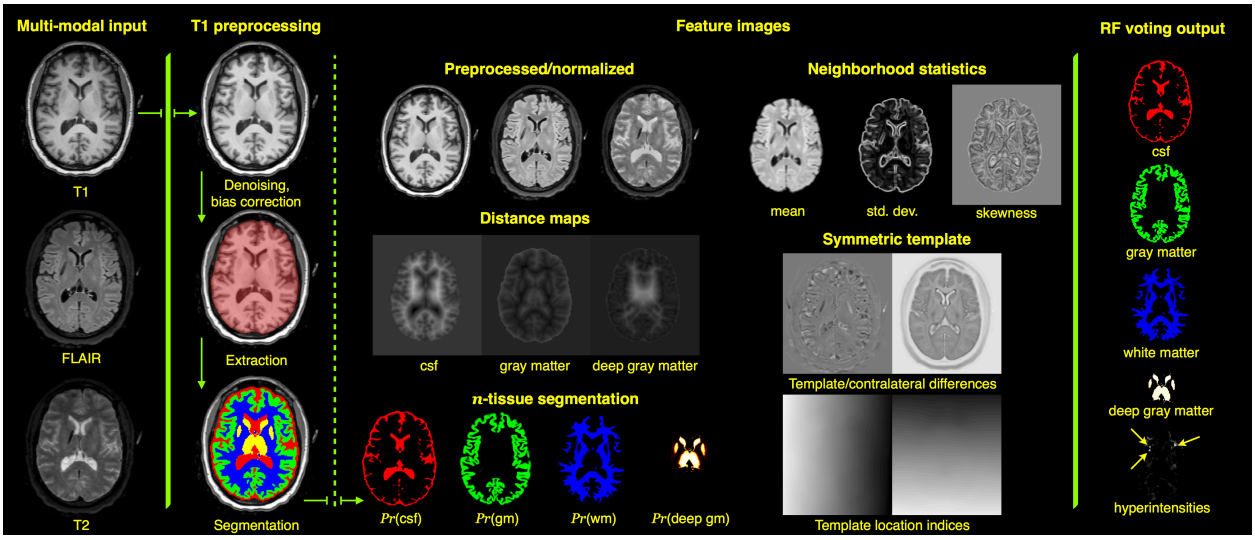

Figure 1: Representation of Stage 1 feature images for subject 01C1019. Input for each subject consists of FLAIR, T1-, and T2-weighted images which are rigidly pre-aligned [6] to the space of the T1 image. The three images are then preprocessed (N4 bias correction [7] and denoising [8]) followed by application of standard ANTs brain extraction and n-tissue segmentation protocols using the MMRR symmetric template corresponding and priors [9] to the T1 image. The feature images are then generated for voxelwise input to the RF model which results in the voting maps illustrated on the right which gives a probabilistic classification of tissue type.

Figure 2: Average `MeanDecreaseAccuracy` plots generated from the creation of all 24 random forest models for both Stage 1 and Stage 2 during the leave-one-out evaluation. These plots are useful in providing a quantitative assessment of the predictive importance of each feature. The error bars provide the 95ˆ{th} percentile (i.e., $1.96 \times sigma$) and illustrate the stability of the feature importance across models.

References

1. Available at http://mlmi2015.web.unc.edu

2. Bauer, S., Nolte, L.-P., and Reyes, M. "**Fully Automatic Segmentation of Brain Tumor Images Using Support Vector Machine Classification in Combination with Hierarchical Conditional Random Field Regularization**" *Med Image Comput Comput Assist Interv* 14, no. Pt 3 (2011): 354–61.

3. Tong, T., Wolz, R., Gao, Q., Guerrero, R., Hajnal, J. V., Rueckert, D., and Alzheimer's Disease Neuroimaging Initiative. "**Multiple Instance Learning for Classification of Dementia in Brain MRI**" *Med Image Anal* 18, no. 5 (2014): 808–18. doi:10.1016/j.media.2014.04.006

4. Liu, X., Tosun, D., Weiner, M. W., Schuff, N., and Alzheimer's Disease Neuroimaging Initiative. "**Locally Linear Embedding (LLE) for MRI Based Alzheimer's Disease Classification**" *Neuroimage* 83, (2013): 148–57. doi:10.1016/j.neuroimage.2013.06.033

5. Neema, M., Guss, Z. D., Stankiewicz, J. M., Arora, A., Healy, B. C., and Bakshi, R. "**Normal Findings on Brain Fluid-Attenuated Inversion Recovery MR Images at 3T**" *AJNR Am J Neuroradiol* 30, no. 5 (2009): 911–6. doi:10.3174/ajnr.A1514

6. Avants, B. B., Tustison, N. J., Stauffer, M., Song, G., Wu, B., and Gee, J. C. "**The Insight ToolKit Image Registration Framework**" *Front Neuroinform* 8, (2014): 44. doi:10.3389/fninf.2014.00044

7. Tustison, N. J., Avants, B. B., Cook, P. A., Zheng, Y., Egan, A., Yushkevich, P. A., and Gee, J. C. "**N4ITK: Improved N3 Bias Correction**" *IEEE Trans Med Imaging* 29, no. 6 (2010): 1310–20. doi:10.1109/TMI.2010.2046908

8. Manjón, J. V., Coupé, P., Martí-Bonmatí, L., Collins, D. L., and Robles, M. "**Adaptive Non-Local Means Denoising of MR Images with Spatially Varying Noise Levels**" *J Magn Reson Imaging* 31, no. 1 (2010): 192–203. doi:10.1002/jmri.22003

9. Tustison, N. J., Cook, P. A., Klein, A., Song, G., Das, S. R., Duda, J. T., Kandel, B. M., Strien, N. van, Stone, J. R., Gee, J. C., and Avants, B. B. "**Large-Scale Evaluation of ANTs and FreeSurfer Cortical Thickness Measurements**" *Neuroimage* 99, (2014): 166–79. doi:10.1016/j.neuroimage.2014.05.044